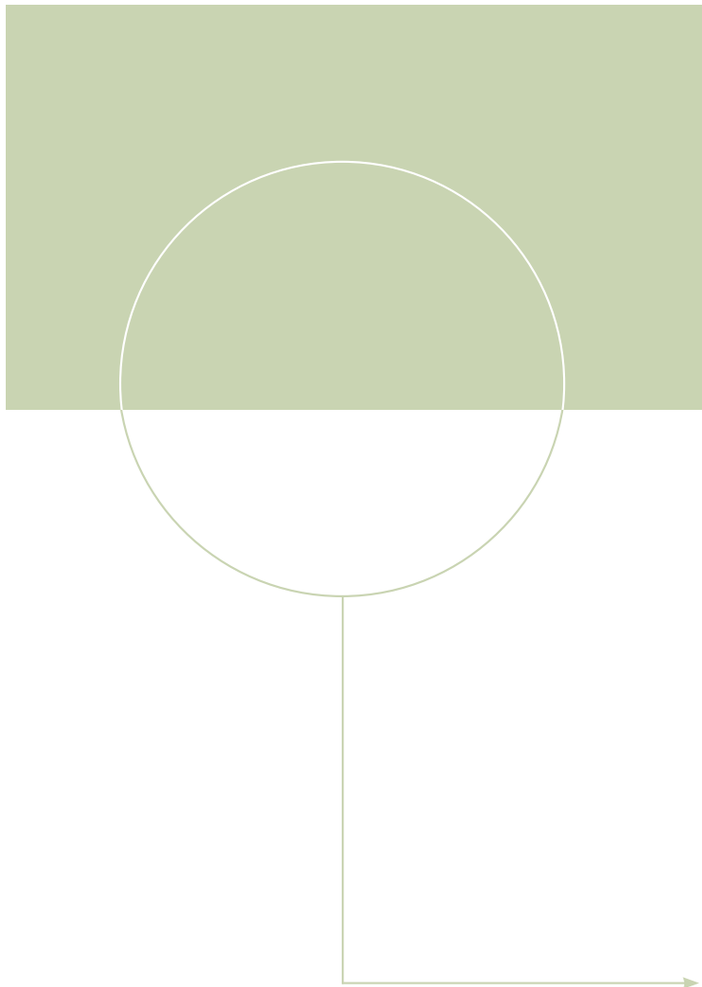

Master's thesis

2020

Robert Nicolai William Balfour

NTNU
Norwegian University of
Science and Technology
Faculty of Natural Sciences
Department of Physics

Robert Nicolai William Balfour

The detection of Meteoric Smoke Particles with rocketborne sensors: A feasibility study

May 2020

NTNU
Norwegian University of
Science and Technology

NTNU
Norwegian University of
Science and Technology

NTNU

Norwegian University of
Science and Technology

The detection of Meteoric Smoke Particles with rocketborne sensors: A feasibility study

Robert Nicolai William Balfour

MLREAL

Submission date: May 2020

Supervisor: Patrick Joseph Espy

Co-supervisor: Michael Gausa

Norwegian University of Science and Technology
Department of Physics

Table of Contents

Abstract

The overarching goal of this master thesis is to explore the feasibility of sending a sensor aboard a rocket to detect Meteoric Smoke Particles (MSP) in the mesosphere, in order to determine their composition. This thesis contributes to the overarching goal by reviewing various sensors capable of identifying, detecting and measuring Meteoric Smoke Particles on the nanometer scale, in the mesosphere. Meteoric Smoke Particles are thought to be the most likely condensation nuclei in the mesosphere for Noctilucent Clouds (NLC). These are high altitude clouds that appear close to the poles during the polar summer. These particles are thought to affect or even be the cause of a number of middle atmospheric phenomena, including noctilucent clouds, polar mesospheric summer echoes, metal layers, charge balance and heterogeneous chemistry, but little is known about these particles. Indeed, their existence is yet to be confirmed by direct measurement, as the mesosphere is home to some of the most severe conditions measured in the atmosphere, including the coldest temperatures, whilst the Meteoric Smoke Particles are thought to be on the nanometer scale. The harsh conditions combined with the small size of the particles means that for a sensor to be able to detect the Meteoric Smoke Particles, it will have to be robust enough to both deal with the conditions of the mesosphere, and sensitive enough to measure particles close to 1 nm in radius, at the same time. Previous attempts at detecting and measuring the Meteoric Smoke Particles have either failed, been inconclusive or only measured the charged part of the particles. Various models have also been used to try to predict their behaviour, whilst indirect observations have also been conducted.

1 Introduction

The mesosphere is a region in the atmosphere, where a number of interesting phenomena occur. In particular, there are clouds that form close to the poles, called noctilucent clouds. These particular clouds should not be able to form so high up in the atmosphere, as the mesosphere is a relatively dry region. Furthermore, the temperatures in the mesosphere should not be sufficiently low enough to reach supersaturation, the levels necessary for homogeneous nucleation, or spontaneous condensation of water vapour, without a pre-existing nucleus (Megner, 2008).

This leads to the need for a pre-existing nucleus, and this is most likely formed through interaction with material either stemming from below or from above the mesosphere. The stratosphere, the region below the mesosphere, has a positive temperature gradient, which suppresses convection and vertical movement, making upward transport unlikely. Thus the natural conclusion is that this material must most likely come from above. Although convection has been observed in the mesosphere, it is too small to explain the aerosols. As this region has a limited input of material from the Earth, it is almost impossible to know what these nuclei consist of. Candidates including ion clusters (Witt, 1969, in Megner, 2008), particles of meteoric origin (Hunten et al., 1980), soot particles (Pueschel et al., 2000, in Megner, 2008) and sulphate aerosols (Mills et al., 2005, in Megner, 2008), have all been suggested. Out of these, re-condensed meteoric material has long been considered the most likely (Megner, 2008). As a result, a

consensus has been reached amongst scientists, that meteoric material plays a key role in a number of different middle atmospheric phenomena, including noctilucent clouds, polar mesospheric summer echoes, metal layers, charge balance and heterogeneous chemistry. Furthermore, the effect of the material is not only restricted to the region where meteoroids ablate, the process where meteoroids lose mass through heating, but also affects processes in the underlying atmosphere and around the globe. Despite the scientific interest, the resulting effects of meteoric material in the atmosphere is not well known (Megner, 2008). Perhaps even more surprising is the lack of unambiguous experimental evidence of their existence. This is mainly due to the tiny dimensions of the particles, as the typical radii are thought to be 1 to 2 nm. Consequently, only measurements of the charged fraction have so far succeeded, and these do not yet yield a conclusive picture (Schulte and Arnold, 1992; Gelinas et al., 1998; Croskey et al., 2001; Lynch et al., 2005, in Rapp & Thomas, 2006).

As we can see from this brief introduction to the topic, the main issue is to find a sensor capable of detecting particles on the nanometer to sub-nanometer scale, whilst also being capable of operating under rocket-flight and mesospheric conditions. Subsequently, the aim of this thesis is to explore the feasibility of sending a sensor aboard a rocket to detect Meteoric Smoke Particles (MSP) in the mesosphere, in order to determine their composition. A literature review looking at the most current research on the MSP was conducted prior to this master thesis, providing valuable background information about the MSP, size estimates, the most likely candidates for the MSP, their location, their charge, and various models on how the MSP behaves. Subsequently, parts of the introduction, theory and methodology chapter will be similar or identical to some parts of the literature review for the sake of continuity and completeness.

This thesis will look at different types of sensors and different operating techniques. The original idea was to use a pyroelectric energy sensor to measure the energy of the MSP. However, these sensors were not sensitive enough to measure the small energy of the MSP, leading us to consider other options. Among them was the condensation particle counters (CPC), the most promising candidate, as it had already been shown to measure particles close to 1 nm in radius (Hering et al, 2017).

Furthermore, this thesis will help fill a gap in the current knowledge on sensors and their feasibility of detecting MSP. If this thesis has a positive result, the possibility of measuring the MSP will be enhanced and might be used to finally detect the MSP, and discern their properties. This in turn could lead to a better understanding of the various phenomena in the middle atmosphere and could be a breakthrough in atmospheric physics.

This thesis will first provide theoretical background information on the MSP and the mesosphere, before relating the methods used for this research and how the sensors were selected. After the methodology section, the thesis will look at previous attempts to detect and measure the MSPs, followed by an assessment of various sensors, including pyroelectric energy sensors and condensation particle counters, before reviewing other instruments that can measure nanoparticles. This is followed by a discussion of the results, a summary of the prominent findings and a suggestion for the way forward.

2 Theoretical background

This section will provide the reader with the theoretical background needed to fully understand the situation and conditions of the MSP in the mesosphere. This section is based on the most prominent findings from the literature review, as the aim of the review was to provide crucial background information on the mesosphere and the MSP. First, a common way of dividing the atmosphere into layers based on temperature gradients will be presented, before going into why the mesosphere is an area of interest and why the mesopause heralds a change in atmospheric conditions. Furthermore it will look at the origin of the MSP, and some of their properties.

2.1 Atmospheric Layers

In atmospheric science, the atmosphere is traditionally split into different altitude regions depending on the temperature gradient (Figure 1). These layers have different properties and chemistry, and are called the troposphere, the stratosphere, the mesosphere, the thermosphere and the exosphere. The lowest region, the troposphere, starts at sea level and goes up to an altitude of 18 km, where the tropopause starts. This is the region which hosts our everyday weather and the majority of the clouds and water vapour. The troposphere is characterised by a decrease in temperature with height and reaches a temperature minimum of approximately -60 °C at the tropopause. Above the tropopause, the temperature starts rising again, mainly due to the ozone layer which absorbs ultraviolet sun light and thus locally heats the atmosphere. The absorption of UV light by the ozone layer represents a local heat source, otherwise the temperature would continue to decrease with height. This region, the stratosphere, goes from the end of the tropopause, around 20 km, to about 50 km of altitude, where the mesosphere begins. Airplanes that can reach high altitudes, can fly in the lower stratosphere and unmanned balloons can reach the middle stratosphere (Megner, 2008; Andrews, 2010; UCAR, 2008).

Above the ozone layer, in the mesosphere, the temperature starts decreasing with altitude once again, primarily due to decreasing absorption of solar radiation by the rarefied atmosphere and increasing cooling by CO_2 radiative emission. The mesosphere extends up to an altitude of about 85-90 km, and is bounded by the mesopause, the coldest region in the entire atmosphere (Megner, 2008). The temperature in the polar summer mesopause can reach below -140 °C (Megner, 2008; NASA, 2000). Only rockets can reach this remote region, making in-situ investigations technically challenging and very costly (Megner, 2008). In-situ observations of the mesosphere are therefore sparse compared to the lower atmosphere, and even though satellite and lidar-observations have provided substantial information, there are many processes and phenomena that are not yet fully understood. One of these processes is the formation of ice particles at very low water concentrations (Megner, 2008). After the mesopause we have the thermosphere, where the temperature starts rising again, this time due to absorption of high energy solar radiation, mainly from short wavelength UV- and soft X-ray radiation, by the small amounts of nitrogen, oxygen and other species remaining at these altitudes. The thermopause, also known as the exobase, is the layer between the thermosphere and the exosphere. The altitude boundary of the thermosphere varies

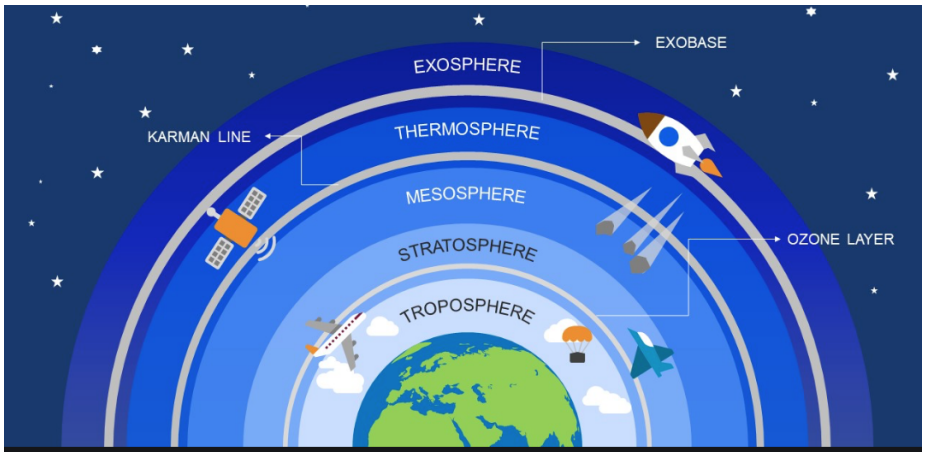

Figure 1: A model of the atmosphere, illustrating the different layers (SlideModel, 2019).

with solar activity. At high solar activity, around the peak of a sunspot cycle, X-rays and ultraviolet radiation from the Sun heats up the thermosphere, raising the altitude of the thermopause to about 1000 kilometers above the Earth's surface (UCAR, 2011). When the Sun is less active during the low point of a sunspot cycle, solar radiation is less intense and the thermopause recedes to within around 500 km of the Earth's surface (UCAR, 2011).

Finally, we have the exosphere. The exosphere is the uppermost region of Earth's atmosphere and it gradually fades into the vacuum of space. Air in the exosphere is extremely thin, consisting primarily of hydrogen and helium, and in many ways it is almost the same as the airless void of outer space. One definition places the uppermost edge of Earth's atmosphere at around 190 000 kilometers of altitude, about halfway to the Moon. At this distance, radiation pressure from sunlight exerts more force on hydrogen atoms than the pull of Earth's gravity does. Not all scientists agree that the exosphere is really a part of the atmosphere. Some scientists consider the thermosphere the uppermost part of Earth's atmosphere, and see the exosphere as a part of space. However, for this thesis, it does not matter whether the exosphere is a part of the atmosphere or not, as it is mainly the mesosphere that is of interest for the MSP. This is a simplified way of defining the atmospheric layers with altitude, as the altitude for the different layers vary with latitude and season. The layer we will mostly be discussing in this thesis will be the mesosphere and the mesopause, as this is the region were MSP are thought to ablate, which is discussed further in section 2.3 (UCAR, 2011;2008; Andrews, 2010; Megner, 2008; NASA 2000).

2.2 The Mesosphere and the Mesopause

The mesosphere is a layer of interest in the atmosphere for a number of reasons, including the phenomena of noctilucent clouds and polar mesospheric summer echoes. How-

ever, the particular altitude range makes the mesosphere difficult to study, as weather balloons and other aircraft cannot fly high enough to reach the mesosphere, whilst satellites orbit above the mesosphere and cannot directly take measurements of this layer. In-situ observations are made using instruments on sounding rockets to sample the mesosphere directly, but such flights are brief and infrequent, not to mention expensive and time consuming. Since the only way to measure the mesosphere directly is through sounding rockets, and these are flown on an infrequent basis, much about the mesosphere is still unknown (UCAR, 2008).

The stratosphere and the mesosphere are often referred to as the "middle atmosphere". This region is different from the lower atmosphere in many ways, as it is less dense and out of reach of convection, so that air parcels do not regularly come in contact with the Earth's surface. Furthermore, the transport is driven in a different way, and it is much dryer, since the moist air that enters this region comes in through the cold tropical tropopause, where the majority of the water is condensed, thus leaving the air with water mixing ratio on the order of parts per million (ppm). To compare, the air with water mixing ratio in the troposphere is on the order of parts per thousand, whilst at the surface and up to 3 km, it is on the order of part per hundred (Megner, 2008; Plane, 2012). According to Plane (2012), hydration thermodynamics indicate that ice nucleation should occur at a temperature around 140 K for a water mixing ratio of 4 ppm, typical of the polar summer mesosphere where NLCs form.

In the middle atmosphere, the exponential decrease of density with altitude continues, resulting in very thin air, which causes larger particles to rapidly sediment out of this region. The middle atmosphere can therefore only host very small particles for any length of time. Nevertheless, the influence of particles in the middle atmosphere is important. During the last decades, it has been shown that particles influence both the charge balance and the chemistry of the middle atmosphere. These particles also enable ice formation in this very dry region, giving rise to very high altitude clouds and sporadic radar echoes, two phenomena of interest in the mesosphere (Megner, 2008).

Furthermore, the mesosphere is collocated with the D-region in the ionosphere, the lowest portion of the partially ionized plasma blanket that surrounds the Earth. (Varney & Kelley, 2015). The ionosphere is a region of the atmosphere that is ionized by solar radiation. The ionosphere increases in thickness and moves closer to the Earth during daylight and rises at night allowing certain frequencies of radio communication a greater range. During daytime hours, it stretches from approximately 50 to 1000 km and includes the mesosphere, thermosphere, and parts of the exosphere. However, ionization in the mesosphere largely ceases during the night, leading to the recombination of ions and electrons. At lower altitudes, where the collision frequency is higher due to the higher densities, the ionosphere is largely neutralized. This causes the lower boundary of the ionosphere to rise to 100 km at night. It has practical importance because it influences, for example, radio propagation on Earth (Speight, 2017).

Various types of waves and tides in the atmosphere influence the mesosphere. These waves and tides carry energy from the troposphere and the stratosphere upward into the mesosphere, driving most of its global circulation (UCAR, 2008).

At the mesopause and below, gases made of different types of atoms and molecules are thoroughly mixed together by turbulence in the atmosphere. Above the mesosphere, in the thermosphere and beyond, gas particles collide so infrequently that the gases be-

come separated based on the chemical elements they contain (UCAR, 2008). This is called the turbopause, and it marks the altitude in an atmosphere below which turbulent mixing dominates. Mathematically, it is defined as the point where the coefficient of eddy diffusion is equal to the coefficient of molecular diffusion. The region below the turbopause is known as the homosphere, where the atmosphere is well mixed for chemical species which have long mean residence times. Highly reactive chemicals tend to have variable concentration throughout the atmosphere, while nonreactive species have more homogeneous concentrations. The region above the turbopause is the heterosphere, where molecular diffusion dominates and the chemical composition of the atmosphere varies according to chemical species and their atomic weight. In other words, the atmospheric gases are not well-mixed above this layer (Atreya, 1986). Furthermore, in the upper atmosphere, the effects of ionisation become dominant in determining the atmospheric dynamics and the air becomes so rarefied that the assumption that it can be treated as a continuous fluid starts to break down (Andrews, 2010).

These changes herald a change in atmospheric conditions, and looking at the figures provided by NRLMSISE-00 confirms some of these changes (NASA, 2000). NRLMSISE-00 is an empirical, global reference atmospheric model of the Earth from ground to space. It models the temperatures and densities of the atmosphere's components. A primary use of this model is to aid predictions of satellite orbital decay due to atmospheric drag. This model has also been used by astronomers to calculate the mass of air between telescopes and laser beams in order to assess the impact of laser guide stars on the non-lasing telescopes. The model is based on the earlier models MSIS-86 and MSISE-90, but updated with satellite drag data. It also predicts anomalous oxygen (Picone et al., 2002).

The acronym is split into several parts. NRL is short for the US Naval Research Laboratory, while MSIS is the acronym for mass spectrometer and incoherent scatter radar, which are the two primary data sources for development of earlier versions of the model. E indicates that the model extends from the ground and through the exosphere and 00 is the year of release. Over the years, NRLMSISE-00 has become the industry standard for international space research (Picone et al., 2002).

This model lets you plot the temperatures and densities of the atmosphere's components for dates between 1960 to 2020. Using this model and creating various plots for different altitude regions and seasons can inform us about the atmosphere (NASA, 2000). Figures 2, 3 and 4 were created by setting the date to 1st of January, year 2000 at 55° of latitude and 45° of longitude, with the hour of day set to 1.5 at universal time.

Plotting from 70 to 120 km of altitude with a stepsize of 1 km, it is easy to see that there is a peak of atomic oxygen at an altitude around 97 km, the same area where it is the coldest, according to the figures. After this maximum in atomic oxygen and minimum in temperature, we can see that the trend starts to turn, as the temperature starts increasing with altitude, and the atomic oxygen starts decreasing. Another interesting point from the figures is that the total mass density is decreasing exponentially with altitude, even though there is a peak in atomic oxygen, as atomic oxygen is still a minor species. This means that the collision rate will decrease with altitude, as the

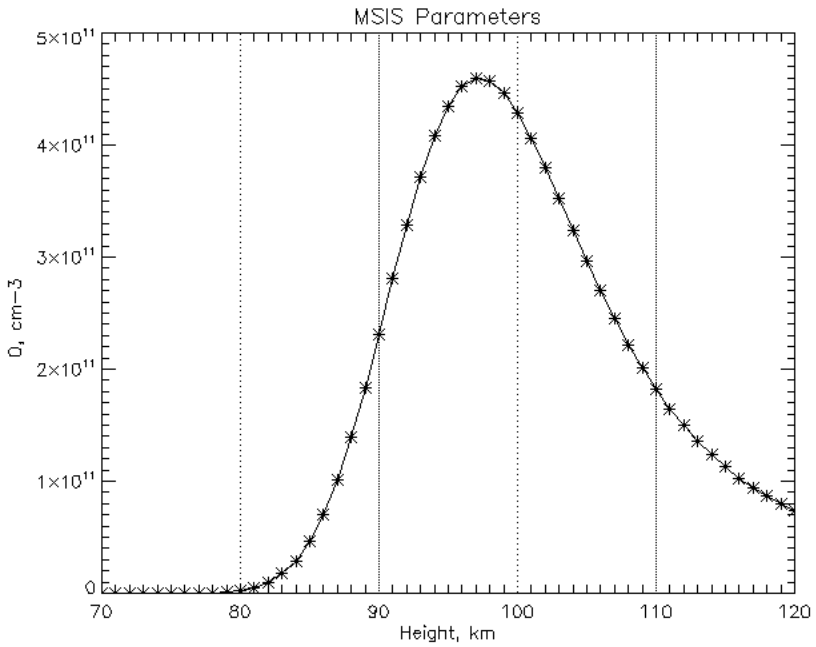

Figure 2: A graph showing the density of atomic oxygen between the altitude of 70 to 120 kilometers on January 1st, 2000 at 55° of latitude and 45° of longitude (NASA, 2000). In the figure, the density of atomic oxygen increases from 80 km, until it reaches a maximum at around 97 km, before starting to decrease again. The increase in atomic oxygen is due to UV radiation splitting oxygen molecules into atomic oxygen. The decrease of atomic oxygen above 97 km is due to the restricting factor of decreasing density of oxygen.

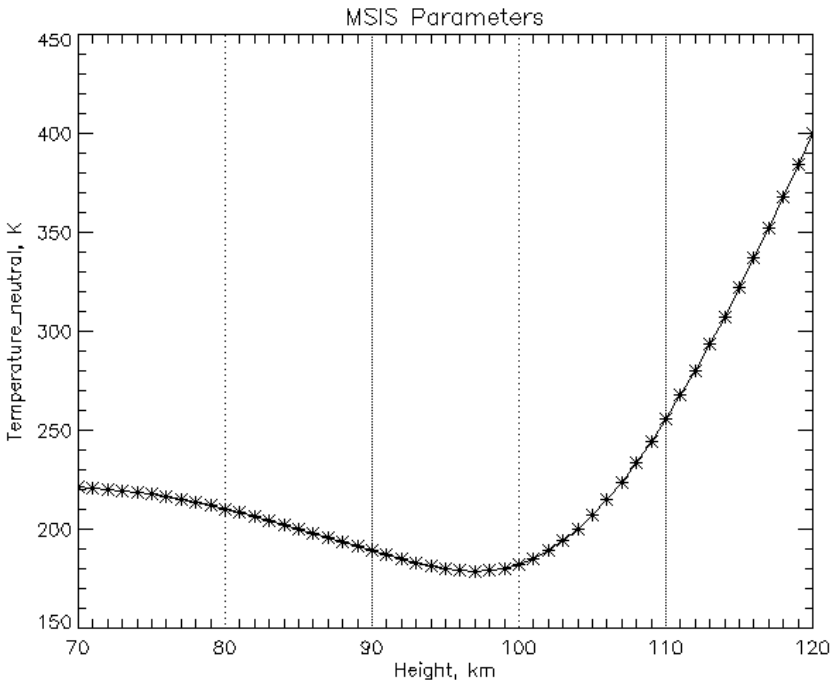

Figure 3: A graph showing the temperature of the atmosphere between the altitude of 70 to 120 kilometers on January 1st, 2000 at 55° of latitude and 45° of longitude (NASA, 2000). The temperature decreases with altitude before it reaches a minimum at the mesopause. After the mesopause, the temperature starts increasing again due to absorption of high energy UV- and soft X-ray radiation by the small amounts of nitrogen, oxygen and others species remaining at these altitudes.

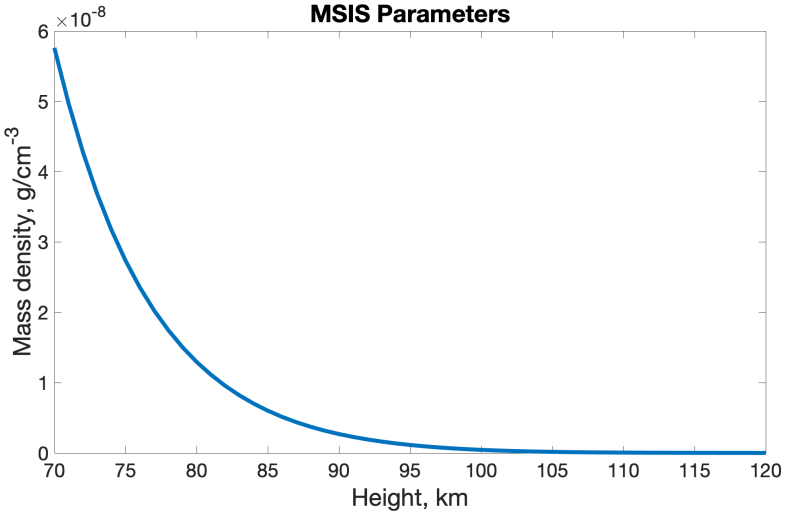

Figure 4: A graph showing the total mass density of the atmosphere between the altitude of 70 to 120 kilometers on January 1st, 2000 at 55° of latitude and 45° of longitude (NASA, 2000). The total mass density decreases exponentially with altitude, as the density of the various components of the atmosphere decrease with altitude.

collision rate in collisions/m^3/s is proportional to number densities and temperature:

$$Z = n_A n_b \sigma_{AB} \sqrt{\frac{8k_B T}{\pi \mu_{AB}}} \tag{1}$$

where n_A is the number density of molecule A in the gas, n_B is the number density of molecule B in the gas, σ_{AB} is the reaction cross section (the area where two molecules collide with each other), k_B is Boltzmann's constant, T is the temperature and μ_{AB} is the reduced mass of the reactants A and B. The reaction cross section σ_{AB} can be simplified to $\sigma_{AB} = \pi(r_a + r_b)^2$, where r_a and r_b is the radius of A and B respectively. Although the temperature does start to increase after 97 km, the collision rate is more dependent on the number densities, meaning that the collision rate will still decrease, even though the temperature is increasing. Thus, the mesopause heralds a change in the atmospheric conditions.

2.3 Origin of the Meteoric Smoke Particles

Meteoric smoke particles originate from meteoroids entering the Earth's atmosphere at high velocities between 11 to 72 km/s (Plane, 2015). During the descent through the atmosphere, the meteoroids experience strong deceleration, and undergo rapid frictional heating by colliding with air molecules. This causes the meteoroid to be ionized and ablated, and subsequently chemical reactions occur with the surrounding air, which in turn makes the meteoroid glow, both in the head and the trail. This results in what we

call a meteor. If the particles in the meteor reach the melting point ($\sim$ 1800 K), their constituent minerals will rapidly vaporize. This process is known as meteoric ablation (Plane, 2012). At this stage, the meteor will shine brightly due to the heat caused by the deceleration and the start of the ablation process. Ablation refers to mass loss of any form, such as erosion, evaporation or melting, and tends to occur where the atmospheric pressure is around 1 μbar. This means that close to 90 km, the peak ablation rate occurs (Plane, 2012). The very small meteoroids, typically smaller than 10 μm, have a large surface area relative to their mass, enabling them to cool efficiently. These particles can, therefore, survive the impact of the atmosphere without ablating, and are referred to as micrometeorites. Larger meteoroids do not always fully ablate, in which case the part that survives the atmospheric entry can be found on the ground, and is known as a meteorite (Megner, 2008). The estimates of how much meteoric material that enters the Earth's atmosphere varies from 5 to 270 tonnes per day (Love & Brownlee, 1993; Nesvorny, 2009, in Plane, 2012). There are two main reasons for the uncertainties in the estimates. The first reason is the problems involved in measuring the meteoric influx, and the second reason is that different measurement techniques are sensitive to different size ranges of incoming meteoroids. In studies related to the MSP, only the ablated meteoric material that stays in the atmosphere is of interest. In atmospheric studies we can, therefore, neglect the mass influx of micrometeorites, as they are not deposited in the atmosphere. Furthermore, the remaining mass of large meteoroids (>1m) that have not fully ablated, can also be neglected. The parts of these large meteoroids that have ablated, will contribute to the meteoric mass influx, and will have to be included. As far as atmospheric studies are concerned, it is therefore enough to consider the mid-range of the meteoroid mass spectrum (Megner, 2008). Within the remaining size range of meteoroids, the mass distribution peaks around 10^{-5} g (Flynn, 2002, in Megner, 2008), and as much as 80% of the incoming mass originate from meteoroids of sizes between 10^{-7} g and 10^{-3} g (von Zahn, 2005, in Megner, 2008). Hence, for atmospheric studies, it is enough to consider this mass range. Still, estimates of the mass flux within this mass range varies with almost an order of magnitude (Gabrielli et al., 2004; Love & Brownlee, 1993; Mathews et al., 2001, in Megner, 2008; Ceplecha et al., 1998; Plane, 2012).

At which altitude ablation happens depends on the speed, size, entry angle, and composition of the meteoroids (Ceplecha et al., 1998). Subsequently, faster meteoroids experience stronger deceleration and therefore ablate at higher altitudes (Megner, 2008). Furthermore, most of this material is thought to be ablated and vaporized in the 70-120 km altitude region (Hunten et al., 1980; Kalashnikova et al., 2000; Plane, 2004; Janches & ReVelle, 2005, in Megner, 2008). The subsequent chemical conversion, re-condensation and coagulation of this evaporated material is thought to form nanometer sized meteoric smoke particles. They are then subject to further coagulation, sedimentation and global transport by the mesospheric circulation.

MSPs have been proposed as a key player in the formation and evolution of ice particle layers around the mesopause region, and in particular noctilucent clouds and polar mesosphere summer echoes, described in previous sections. MSPs have also been implicated in mesospheric heterogeneous chemistry to play an important role in the mesospheric charge balance (Rapp & Lübken, 2001; Rapp, 2009; Friedrich et al., 2011, in Hedin et al., 2014), to be a significant component of stratospheric aerosol and

enhance the depletion of ozone (O_3) (Murad et al., 1981; Curtius et al., 2005; Voigt et al., 2005, Saunders et al., 2012, in Hedin et al, 2014).

The surviving meteorites indicate what meteoric material is made of. Although it varies with the origin of the meteoroid, the seven predominant substances are; Fe, Na, Mg, Si, Ca, Al and Ni (Ceplecha et al., 1998). The general composition of the meteoric smoke material is thought to reflect the composition of the incoming meteorite material. However, due to differential ablation processes, and the altitude-dependent chemical environment, the detailed smoke composition is expected to depend on the history of the individual meteoric particles (Hedin et al, 2014).

2.4 Properties of the MSP

This section will summarize the properties of the MSP found by the literature review. The size estimates of the MSP have since 1961 been considered to be on the nanometer scale (Rosinski & Snow, 1961). More recent results and calculations provide a characteristic radius of roughly 1 nm for the particles (Rapp & Thomas, 2007; Megner, 2008; Robertson et al., 2014; Plane et al., 2015). The estimated number densities of the MSP varied greatly. Strelnikova et al. (2007) found number densities rising from ca 10 cm^{-3} at 85 km to ca 1000 cm^{-3} at 90 km, whereas Fentzke et al. (2009; 2012) found densities rising from ca 300 cm^{-3} at 80 km to ca 20,000 cm^{-3} at 94 km. Robertson et al. (2014) found number densities for both positively and negatively charged MSPs to be approximately 2000 cm^{-3} for the 500–2000 atomic mass unit (amu) range at 60-70 km of altitude. Their charge model also indicated that the total number of MSPs is about 10 times the number density in either sign of charge; hence the data together with the charge model indicated a total number density of about 20,000 cm^{-3} in this range of masses and altitude. By including the 0–500 amu mass range, the number density could be doubled if the majority of these particles are MSPs, instead of "ordinary" molecular ions. The model also showed a maximum in the number density at about 84 km. Furthermore, they discovered that MSPs above $\sim$ 80 km are all negatively charged, whilst both charge states occur below 80 km. Finally, MSP charge densities were measured to be lower during the daytime than the nighttime (Robertson, et al., 2014).

Recently, Hervig et al. (2012) provided the first observational evidence that ice particles made by noctilucent clouds, contain small amounts of meteoric smoke particles, about $0.01-3\%$ by volume in the ice particles. They used the Solar Occultation For Ice Experiment (SOFIE) from the Aeronomy of Ice in the Mesosphere (AIM) satellite (Russell et al., 2009, in Hervig et al., 2012), to study the extinction due to NLCs at four wavelengths from the UV to the mid-IR (0.330, 0.867, 1.037, and 3.064 μm) and showed that the extinction was inconsistent with pure H_2O ice particles. Instead, they proposed that the extinction could be explained in terms of the extinction simulated for a mixture of ice and MSPs. They made simulations of 25 different MSP compositions for the ice-smoke mixtures, and out of these, only three of the compositions where consistent with the NLC observations. These were carbon (C), wüstite (FeO), and magnesiowüstite ($Mg_xFe_{1-x}O$, $x = 0.1-0.6$) (Hervig et al., 2012).

Observational evidence for the composition of MSPs was absent prior to Hervig et al (2012). Previous measurements of meteoric remnants in the middle atmosphere, that were much larger than MSPs, suggested compositions of hematite (Fe_2O_3) (Bohren

and Olivero, 1984, in Hervig et al., 2012) and olivine (Mg_2SiO_4 or Fe_2SiO_4) (Klekociuk et al., 2005, in Hervig et al., 2012). Furthermore, laboratory experiments have indicated MSP compositions of hematite, goethite (FeOOH), fayalite (Fe_2SiO_4), and silica (SiO_2) (Saunders and Plane, 2006, in Hervig et al., 2012). While none of these compositions are consistent with the findings in Hervig et al. (2012), the previous suggestions are similar in that iron, magnesium, and oxygen are all present.

Although this result is interesting, it is not conclusive evidence for the MSP composition for a number of reasons. It is unknown whether only MSPs of certain compositions are captured by ice particles, if MSPs undergo chemical changes when incorporated into ice, or if MSP composition changes with season or altitude. The presence of MSPs within NLC ice particles is an intriguing result with respect to the question of mesospheric ice nucleation, as it has long been suggested that MSPs serve as ice condensation nuclei for NLCs. However, the presence of MSPs in ice does not necessarily identify MSPs as the ice condensation nuclei involved in NLCs. The measured content of MSPs in ice appears to exceed what is expected for NLC particles containing a single ice nuclei. This could suggest that each ice particle collects many MSPs, perhaps through coagulation. On the other hand, it is also possible that an ice particle is nucleated by a single MSP, and that many smaller MSPs are subsequently collected through coagulation. According to Turco et al. (1982), MSP must be larger than 10 to 15 Å, or 1 to 1.5 nm in radius to be effective as cloud condensation nuclei. It is also possible to calculate the required radius for a particle to act as a cloud condensation nucleus in the mesosphere, by using Kelvin's equation for water condensation (Andrews, 2010):

$$r = \frac{2\gamma}{\rho_l R_v T ln(e/e_s(T))} \tag{2}$$

where γ is surface tension, ρ_l is density of water, R_v is the specific gas constant for water vapour, T is the temperature, e is the partial pressure of water vapour, and $e_s(T)$ is the saturation water vapour pressure. Numerically, the variables have the following values: γ = 75.65 $\cdot 10^{-3}$ J/m^2 for $T = 0.01$°C (IAPWS, 2014), ρ_l = 977.5 kg/m^3 for $T = -34$°C (Hare & Sorensen, 1987), R_v = 461.5 J/kgK (Lide, 1992), $T = 140$ K (Plane, 2012), and $e_s(T) = 9.397 \cdot 10^{-7}$ Pa for $T = 140$ K (Murphy & Koop, 2005). The partial pressure of water vapour e can be calculated using Dalton's law (Ahmed, 2010): $e_1 = x_1 \cdot e_{tot}$, where x_1 is the mixing ratio and e_{tot} is the total atmospheric pressure. If $x_1 = 4$ ppm (Plane, 2012), and $e_{tot} = 2.142$ Pa at 75 km of altitude (Sissenwine et al., 1968), we get a partial pressure $e = 8.568 \cdot 10^{-6}$ Pa. This results in a radius $r = 1.083746601 \cdot 10^{-9}$ m ~ 1.1 nm. This fits within the size range required for the MSP to act as cloud condensation nuclei, according to Turco et al. (1982). Finally, the amount of MSPs derived from SOFIEs NLC observations is often greater than indicated by MSP models, suggesting another area requiring further investigation (Hervig et al., 2012).

3 Methodology

This section will present the methods and strategies used to identify sensors and instruments capable of measuring nanoparticles, and how their feasibility for detecting the

MSP was determined. As previously mentioned, the overarching goal of the thesis was to find a sensor capable of detecting the MSP in the mesosphere, and these particles are approximately 1 nm in radius. Subsequently, the main method of research has been to identify and review the most current and peer reviewed material regarding sensors, instruments and nanotechnology that can measure nanoparticles. As a result, this thesis aims to present the most recent and noteworthy research in a structured fashion. Furthermore, meetings and correspondence have been conducted with academia and Andøya Space Center, which has been a part of the primary data collection. Secondary data was provided by the aforementioned literature review conducted in the autumn of 2019, which provided much of the theoretical background information.

Concerning the approach, this thesis has a result-driven method behind it, as the sensors considered are disregarded if they do not seem feasible to detect the MSP. The main criteria of feasibility when analyzing the results from the different sensors, that was applied throughout the thesis, was if these were capable of detecting particles close to 1 nm in radius. As a result, the sensors were considered regardless of their method of operation, as long as they could fulfill the main criteria. This is the reason why the sensors reviewed in the thesis differ in terms of operation and functionality. Furthermore, the sensors would be screened according to whether they measured only charged particles or all particles, as the goal of this thesis was to measure all of the particles. Subsequently, sensors that only measured charged particles were disregarded. After being screened, the sensors would have to be modified, in order to solve problems that rocket flight and mesospheric conditions pose, including the time the sensor would need to be able to detect and measure particles. Although only ten different sensors are presented in the thesis, there were more sensors that were initially screened, but deemed unfeasible and thus not included (see Appendix A). These include a micro aerosol sensor for the measurement of airborne ultrafine particles (Zhang et al., 2016) and a technique using dynamic light scattering to measure particles (Kaszuba et al., 2008). The aerosol sensor was deemed unfeasible as the lower cut-off size for particle detection was 50 nm, whilst using dynamic light scattering would require a sample of the MSP, collected from the mesosphere, and this has been proven to be challenging according to Hedin et al. (2014).

4 Previous attempts at detecting and measuring the MSP

This section will briefly present a selection of the previous attempts at measuring and detecting the MSP, elaborate on why they were either unsuccessful or inconclusive, and why measuring the charged part of the particles is easier. As mentioned in the introduction, no unambiguous experimental evidence has so far been reported, although there have been a number of attempts to collect the MSP from the mesosphere (Witt et al., 1963; Kornblum, 1970; Gumbel et al., 2005, in Megner, 2008; Hedin et al., 2014). However, though there have been many successful measurements of charged particles, presumably MSPs, in this region (Gelinas et al., 1998; Horanyi et al., 2000; Lynch et al., 2005; Rapp et al., 2005, in Megner, 2008; Robertson et al., 2014), which can provide insight into number densities and other properties, none have succeeded to determine their composition from direct observations (Megner, 2008; Plane et al.,

2015).

In a recent study, Hedin et al. (2014) attempted to develop a rocketborne instrument, capable of sampling MSPs in the mesosphere and returning them to the ground for detailed analysis in the laboratory. This was part of the Mesospheric Aerosol-Genesis, Interaction and Composition (MAGIC) project. The MAGIC samplers exposed transmission electron microscopy grids in succession, as the payload on the sounding rocket traveled through the upper mesosphere, and were employed on a number of rockets between 2005 and 2011. Hedin et al. (2014) recently discussed the challenges of sampling nanometer-sized particles, in addition to how it affected their subsequent analysis. Particles with compositions close to that expected for MSPs were found, however, uncertainties in the sticking efficiency of the particles on the sampling surfaces, in addition to problems with different types of contamination, rendered the results inconclusive (Plane et al., 2015).

Furthermore, the MSP and ice particles occur at various altitudes, including the D region of the ionosphere, where there are sufficient numbers of free electrons and ions for a significant fraction of the MSP and the ice particles to be charged (Reid, 1990; Havnes et al., 1990; Jensen & Thomas, 1991, in Robertson et al., 2014; Rapp et al., 2007). This has lead to a number of heavy charge carriers being used, to measure the charge in this region.

In 2011, two Charge And Mass of meteoric smoke ParticleS (CHAMPS) sounding rockets were launched into the polar mesosphere, one during the day, the other during the night. They both carried an electrostatic multichannel mass analyzer for charged MSPs, that operated from 60 to 100 km, and returned data on the number density of the charged MSPs in several ranges of mass. Moreover, the payloads carried Faraday rotation antennas, an array of plasma probes for determining electron, ion densities, and the payload charging potential. This provided a comprehensive picture of the distribution of charges over a wide range of altitudes, which could be compared with models for the vertical distribution of MSPs and for the distribution of charge (Robertson et al., 2014).

Another interesting development has been the Existence and Charge state Of meteoric smoke particles in the Middle Atmosphere (ECOMA) particle detector (Plane et al., 2015). The ECOMA particle detector is a Faraday cup instrument, which contains up to three pulsed vacuum ultraviolet (VUV) lamps to photodetach electrons from negatively charged particles or photoionize neutral particles. One significant result was to show that the resulting photoelectron current is proportional to the MSP volume density, and this property has been used to support global modeling predictions regarding the seasonal variability of MSPs (Plane et al., 2015). When the ECOMA detector employs three flashlamps, each lamp has a different window material with a different cutoff wavelength. Using a VUV lamp with a cutoff at 110 nm, produces a much larger photoelectron current in comparison with VUV lamps that have cutoffs at 190 and 225 nm, particularly above 88 km. This data enables constraints to be placed on the MSP size, work function, and composition. For instance, in one of the studies, the particles observed were concluded to be in the 0.5–3 nm size range, increasing in size toward lower altitudes. This is not surprising, as the MSPs are expected to increase in size at lower altitudes due to coagulation. The MSP work function was estimated to be in the range from 4 to 4.6 eV. Electronic structure calculations showed that this low work

function indicated that iron and magnesium oxy/hydroxide clusters, rather than metal silicates, were the major components of the MSPs producing the photoelectron currents measured on this flight (Plane et al., 2015). This particular result matches with the one found by Hervig et al. (2012) in a previous section.

As we have seen in this section, the previous attempts of measuring the MSP have either been unsuccessful, inconclusive or only focused on the charged part of the particles. In this thesis, we are concerned with measuring all of the MSP, not just the charged particles, as we want to grasp the comprehensive picture. Subsequently, in the following sections, we will investigate various alternatives of measuring the MSP in the mesosphere, by utilising different sensors and measurement techniques.

5 Pyroelectric sensor

The original idea of this thesis was to use a pyroelectric sensor to detect and measure the energy of the MSP, and thus determine their composition. The sensor was to be on-board a rocket travelling at speeds between 800 and 1400 m/s, and the sensor was to measure the collisional energy between the rocket and the MSP. One way of calculating this energy is through using the most likely mass of the MSP. As has previously been mentioned, a literature review was conducted prior to this thesis, to provide crucial background information about the MSP. Included in the literature review was a recent article by Herving et al. (2012), that listed the most likely compositions of the MSP, and they have been summarized in this article in table 1. The table is sorted after density, with the most dense substance at the top, followed by the less dense substances. The density of the different substances is interesting, as it is then possible to calculate their mass and their corresponding energy. Fortunately, these compositions have known densities, except for magnesiowuštite, meaning it is possible to find their mass by having their volume, as $m = \rho \cdot V$, where ρ is the density and V is the volume of the MSP. If we assume that the particles are spherical, then the volume V becomes $\frac{4\pi}{3}r^3$, where r is the radius of the MSP. The radius of the MSP has in multiple articles been approximated to be around 1 nm (Rapp et al., 2007; Megner, 2008; Robertson et al., 2014), so it is possible to find the mass of the different compositions. Calculating the mass of olivine and wüstite, we get $m = 1.403244719 \cdot 10^{-23}$ kg for olivine, and $m = 2.46300864 \cdot 10^{-23}$ kg for wüstite. Once we have calculated the mass, it is possible to calculate the collisional energy between the rocket and the MSP, as $E = \frac{1}{2}mV^2$, where V is the velocity of the rocket, and not to be confused with the volume of the MSP. We assume that the particles are at rest, and that the rocket has a velocity of 1400 m/s. We also assume that all of the energy from the rocket is transferred to the MSP on collision. This gives us the following energy for olivine and wüstite respectively: $E = 1.375179824 \cdot 10^{-17}$ J for olivine, and $E = 1.375179824 \cdot 10^{-17}$ J for wüstite.

As table 1 illustrates, wüstite is the most dense material of the suggested MSP compositions, meaning the upper limit for energy detection is $2.413748468 \cdot 10^{-17}$ J ~ 24 aJ. Furthermore, it is unlikely that all of the energy from the rocket is transferred to the MSP on collision, meaning this is very much a best case scenario. Prior to the investigation of different sensors and the results of the energy calculation, we believed that pyroelectric energy sensors would be able to measure the energy of the MSP. We

Composition	Chemical Formula	Density
Wüstite	FeO	5880 kg/m^3
Hematite	Fe_2O_3	5260 kg/m^3
Fayalite	Fe_2SiO_4	4390 kg/m^3
Goethite	FeOOH	4280 kg/m^3
Olivine	Mg_2SiO_4 or Fe_2SiO_4	3350 kg/m^3
Silica	SiO_2	2650 kg/m^3
Carbon	C	2100 kg/m^3
Magnesiowüstite	$Mg_xFe_{1-x}O$, $x = 0.1 - 0.6$	??

Table 1: A table listing the most likely compositions of the MSP (Hervig et al., 2012), ordered by decreasing density (Anthony et al., 2003; Lide, 2005; Haynes, 2011; Guo et al., 2012).

assumed they could measure down to 1 nJ, which is eight orders of magnitude too big. Too further illustrate the problem, we calculated the required radius of wüstite when it has an energy of 1 nJ:

$$E = \frac{1}{2}mV^2 = \frac{1}{2}\rho\frac{4\pi}{3}r^3V^2 \tag{3}$$

Solving with regard to the radius r:

$$r = \sqrt[3]{\frac{3}{2}\frac{E}{\rho V^2\pi}} = 3.46 \cdot 10^{-7} \text{ m} \tag{4}$$

which is two orders of magnitude too big.

According to the editors of Industrial Laser Solutions (2014), the most sensitive pyroelectric energy sensor on the market is the PE9-ES-C, which measures the lowest laser energies in the industry at 50 nJ. This is far off the required sensitivity. Ophir Photonics (2020) claimed on their website that they had a sensor capable of measuring down to the pico joule energy region, but this is still five orders of magnitude higher then the required sensitivity (Ophir Photonics, 2013, 0:56). As this was the most sensitive pyroelectric energy sensor on the market, the conclusion is that it is not feasible with today's pyroelectric energy sensors to measure the energy from the MSP, and thus we started looking at other options.

6 Condensation Particle Counter

After realizing that the pyroelectric sensors were not sensitive enough for the detection of MSP, other types of sensors were considered. Condensation Particle Counters (CPC)

were considered an interesting option, as they have already been proven to be sensitive enough to detect particles close to 1 nm in radius (Hering et al., 2017). Furthermore, their operation seemed feasible on a rocket, as long as it was possible to modify them to work under mesospheric conditions.

This section will first describe how a CPC operates, followed by a review of the modifications and other issues that need to be solved for the sensor to be operable under mesospheric conditions. Finally, we will conclude whether the CPC is a feasible option for detecting and measuring the MSP.

6.1 CPC Concept

The purpose of a CPC, is to use a substance to grow the desired particle to a size where it is measurable. This is done by having an open air flow at the top of the CPC, enabling particles to be sampled. In the CPCs created by Hering et al. (2017; 2019), water was the substance used to grow the sampled particles. Generally, a CPC operates in the following way; firstly the air enters a cool area called the conditioner stage, which is cooler than the incoming air, enabling the water in the air to condense on the surface. The condensed water is then sent to the warm initiator stage, where it is heated to be warmer than the incoming air, allowing evaporation of the liquid water, thus creating supersaturated conditions in the air current. The air current does not become noticeably warmer, as air is a good insulator, and thermal diffusion from the warm initiator wall into the bulk of the air current would be slow. The supersaturated conditions in the initiator activate particles in the air current, and allow the particles to condense the water into droplets. The excess water, the water that did not condense in the air current, is collected in the cooled moderator stage for re-use in the initiator, and the condensed water droplets follow the air current to be optically measured further downstream. To summarize; the conditioner gathers the water vapour from the air, then the initiator releases it back into the air at a concentrated level in order to form droplets, then the moderator gathers the excess water for re-use, whilst the condensed water droplets follow the air current to be optically measured. This is illustrated in figure 5.

There are a number of modifications that will need to be implemented in order to make the CPC operable in the mesosphere. One of the difficulties in the mesosphere is to make the water in the air current condense on the conditioner, as the conditioner must be at a colder temperature than the air current. However, the air current can reach temperatures lower then 140 K (NASA, 2000), resulting in fusion into ice instead of condensation on the conditioner. Because of this, the conditioner stage of the CPC will most likely have to be removed, as it would freeze the water out of the air current, and this cannot be wicked around. Furthermore, the mesosphere is a relatively dry region, meaning there might not be enough water available in the air to form enough ice to make the CPC operable. This might be solved by bringing a water supply for the CPC. This would be wicked into the initiator stage to create supersaturation in the air current, allowing nucleation on particles of a particular size, which depends on the degree of supersaturation. These particles would then be detected optically. Furthermore, the degree of supersaturation would have to be kept below the degree needed for homogeneous nucleation, as the water would then form ice onto itself, and

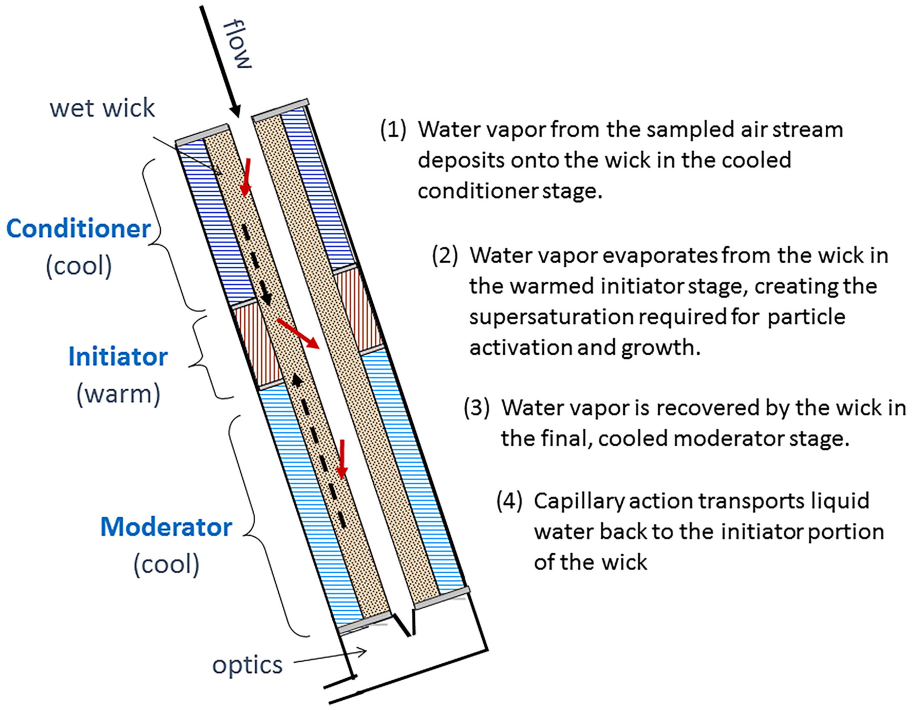

Figure 5: A schematic of the MAGIC CPC, that illustrates the different stages of the CPC and how these operate (Hering et al., 2019).

it would be unfeasible to tell particles formed through homogeneous nucleation apart from those formed on MSP. Finally, the moderator might have to be removed, as it could potentially ice up and block the air current.

6.2 Ice Nucleation

The CPC has a critical radius, or an activation radius, where particles equal to or larger than this radius will nucleate the water into ice, allowing the particle to grow through condensation. This radius is dependent upon the degree of supersaturation in the CPC, and can be described quantitatively by Kelvin's formula, modified for the nucleation of ice (Murray et al., 2012):

$$r = \frac{2\gamma}{\rho_l R_{water} T \ln(S)}, \tag{5}$$

where γ is the surface tension or surface forming energy of ice, ρ_l is the density of water, R_{water} is the specific gas constant for water, T is the temperature and S is the saturation ratio of the ambient water vapour pressure and the saturation vapour pressure over a plane ice surface, and is derived from the ratio of vapour pressures of liquid water

and ice, (p_l/p_{ice}). p_l and p_{ice} can be determined by the following formulas, found in Murphy & Koop (2005):

$$\ln(p_l) \sim 54.842763 - \frac{6763.22}{T} - 4.210\ln(T) + 0.000367T + \tanh(0.0415(T-218.8)) \cdot (53.878 - \frac{1331.22}{T} - 9.44523\ln(T) + 0.014025T) \quad (6)$$

Calculating with their formula, using a temperature of 140 K, we end up with a vapour pressure of $9.397 \cdot 10^{-7}$ Pa for liquid water. For ice, we have:

$$p_{ice} = \exp\left(9.550426 - \frac{5723.265}{T} + 3.53068\ln(T) - 0.00728332T\right) \quad (7)$$

For T = 140 K, we get a vapour pressure for ice of $3.37 \cdot 10^{-7}$ Pa. This gives us a saturation ratio of $S = 2.7884273$.

Nummerically, the other variables have the following values: $\gamma = 77$ mJ/m^2 at $T = -25°$C (Boinovich & Emelyanenko, 2014), T = 140 K (Plane, 2012), $\rho = 977.5$ kg/m^3 at $T = -34°$C (Hare & Sorensen, 1987), $R_{water} = 461.5$ J/kgK (Lide, 1992). This gives us the following radius:

$$r = \frac{2 \cdot 77 \cdot 10^{-3} \text{ J/m}^2}{977.5\text{kg/m}^3 \cdot 461.5 \text{ J/kgK} \cdot 140 \text{ K} \cdot \ln(2.7884273)} \quad (8)$$

which results in a radius $r = 2.377814516 \cdot 10^{-9}$ m ~ 2.38 nm. Particles with a radius equal to or larger than 2.38 nm will nucleate the water into ice, allowing the particle to grow through condensation. As mentioned previously, most of the literature claim that MSP have a characteristic radius of 1 nm (Rapp et al., 2007; Megner, 2008; Robertson et al., 2014; Plane et al., 2015), but the CPC could still measure the larger MSP. Furthermore, there are a number of uncertainties in these calculations, as some of the values are approximations, whilst others are valid for higher temperatures. This could lead to the critical radius of the CPC reaching down to 1 nm. However, if these values are correct, then the required saturation rate for a particle of 1 nm in radius to nucleate water into ice is: $S = 11.45465122$. Fortunately, this degree of supersaturation is most likely lower than that needed for homogeneous nucleation, as the saturation level required seems to increase as the temperature decreases (Viisanen, et al., 1993). However, obtaining this high level of supersaturation in a relatively dry region of the atmosphere is unlikely.

6.3 Condensation Rate

Another point of interest is the condensation rate, as the time the air current is inside the CPC is quite limited. The particles will have to condensate quickly for the optical part of the sensor to be able to detect the particles. If we assume that the length of the CPC is 1 meter, and that the rocket has a speed of 1000 m/s, it will take the air current 1 ms to fly through the CPC. So the question is whether the particles flying through the

CPC will grow large enough to be measured in the optics section, with only 1 ms of growth. Campbell & Bakhtar (1970) have found a formula for calculating the rate of condensation for water. The rate of condensation on to a droplet C_{m} in mass per unit time, can be obtained from the kinetic theory of gases as

$$C_{\mathrm{m}} = \frac{4\pi r^2 pq}{\sqrt{2\pi R T_{\mathrm{G}}}} \tag{9}$$

where r is the radius of a droplet, p is the pressure, q is the condensation effect, R is the gas constant for water vapour and T_{G} is the temperature of the vapour (Campbell & Bakhtar, 1970). If the radius of the droplet is roughly 1 nm, the pressure is the found saturation vapour pressure for water; $9.397 \cdot 10^{-7}$ Pa, q is between 0.45 and unity (Mills & Seban, 1967), R is 461.5 J/kgK for water vapour (Lide, 1992) and T_{G} is 140 K, we get a rate of condensation $C_{\mathrm{m}} = 1.853357868 \cdot 10^{-26}$ kg/s, if $q = 1$. If $q = 0.45$, we get $C_{\mathrm{m}} = 8.340110408 \cdot 10^{-27}$ kg/s.

As the articles concerning the sensors did not provide a cut-off size for particle detection in the optics section, we can instead calculate the time the particles would need to grow bigger. In order to calculate the time needed for a particle to grow from 1 nm to 2 nm in radius, we assume that the particles are spherical with a volume $V = \frac{4\pi r^3}{3}$. It is then possible to use their volume in combination with the mass density of water to find the mass of the particles, as $m = \rho \cdot V$. The mass density of water is ~ 1000 kg/m^3 (Lide, 2003). When we have the mass corresponding to the different radii, we can calculate the difference. Finally, by dividing the mass difference by the condensation rate found using Campbell & Bakhtar's formula (1970), we end up with the time it takes for a particle to grow from 1 nm to 2 nm. For a radius of 1 nm, we get a volume $V_1 = 4.188790205 \cdot 10^{-27}$ m^3, which corresponds to a mass $m_1 = 4.188790205 \cdot 10^{-24}$ kg. For a radius of 2 nm, we get a volume $V_2 = 3.351032164 \cdot 10^{-26}$ m^3, which corresponds to a mass $m_2 = 3.351032164 \cdot 10^{-23}$ kg. The difference between the two, Δm is then: $\Delta m = m_2 - m_1 = 2.932153144 \cdot 10^{-23}$ kg. Dividing by the condensation rate found above, $C_{\mathrm{m}} = 1.853357868 \cdot 10^{-26}$ kg/ms, we get a time:

$$t = \frac{\Delta m}{C_{\mathrm{m}}} = \frac{2.932153144 \cdot 10^{-23}\mathrm{kg}}{1.853357868 \cdot 10^{-26}\mathrm{kg/s}} = 1582.076076 \text{ s}, \tag{10}$$

which is ~ 26 minutes. It will take 26 minutes for a particle to grow from 1 nanometer in radius to 2 nanometers. From this it is clear that the particles will not grow fast enough to be measurable as they enter the optics section of the CPC, leaving the use of a CPC as a potential candidate for detecting MSP, unfeasible.

7 Other sensors

After concluding that the CPC would not be able to measure the MSP, other options were considered. This section will therefore investigate various instruments that are able to measure nanoparticles, including instruments that measure number densities, surface concentrations and mass concentrations.

A list of instruments capable of measuring number densities of nanoparticles can be found in chapter 2 by Bergamaschi et al. (2012), where the details of how the instruments operate and the size range they can detect are provided. The first suggestion was to use a CPC, but as we have seen in the previous section, they are not suited to measure the MSP. The next suggestion was to use an Optical Particle Counter (OPC) to measure nanoparticles, however, they are not sensitive enough to measure the MSP, as they can only detect particles down to a size of 300 nm. Finally, they suggested using a Scanning Mobility Particle Sizer (SMPS), which uses a combination of a Differential Mobility Analyzer (DMA) and a CPC. Once again, the CPC is not suited to measure the MSP, leaving this last option unfeasible. Fortunately, Bergamaschi et al. (2012) suggested other instruments that measure different quantities of nanoparticles. A brief description of the various instruments and their feasibility for detecting and measuring the MSP is given below.

Bergamaschi et al. (2012) suggested four instruments that measure the surface concentration of nanoparticles; Diffusion Chargers (DCs), the Electrical Low Pressure Impactor (ELPI), the Nanoparticle Surface Area Monitor (NSAM) and the Modified Electrical Aerosol Detector (MEAD) (Bergamaschi et al., 2012).

DCs give real-time measurement of aerosol active surface area. The active surface area does not scale with geometric surface area above 100 nm, and the DCs underestimate the surface area of particles larger than 100 nm. For particles smaller than 100 nm, an appropriate inlet pre-separator must be used to enable the DC to measure them. Depending on the model, measurements can be logged every 10 seconds. A recent improvement in DCs is the Diffusion Size Classifiers (DiSCs), which can obtain both the total number density and average particle size. The DiSCs time resolution is about 2 seconds, and they are battery-powered and portable (Bergamaschi et al., 2012). According to Fierz et al. (2008), the DiSC can measure the number concentration and the average diameter of nanometer sized particles in the size range of 10 to 200 nm. Unfortunately, this size range does not suit the MSP. Fierz et al. (2011) have further developed a miniature DiSC, the miniDiSC, but this has an even more limited size range. It seems unlikely that these sensors and instruments will be sensitive enough to detect the MSP.

The ELPI gives real-time size-selective detection of active surface area concentration of particles between 7 nm and 10 μm. It combines electrical charging, inertial collection and electrical detection. The ELPI is a real-time cascade impactor, where particles first pass through a diffusion charger, before subsequently being positively charged. They then enter a Berner-type low pressure impactor made up of 13 stages where the particles are collected onto electrically isolated stages by aerodynamic diameter. The current on each stage, measured by electrometers, is then converted into a particle number concentration. Depending on the model, measurements can be logged every 5 seconds. The offline characterization (TEM, ICP-MS, etc.) of samples is also possible. The restricting factors are the size, expense, complexity of operations and sensitivity to harsh field conditions (Bergamaschi et al., 2012). In particular this last factor might prove to be the most limiting for the ELPI, as the mesosphere has some of the harshest field conditions in the atmosphere. Using the ELPI to detect the MSP, thus seems unfeasible.

The NSAM is based on the widely accepted model by the International Commi-

sion on Radiological Protection (ICRP). It is an instrument aimed at determining lung-deposited particle surface area concentrations (Bergamaschi et al., 2012). The limitation and perspective of this kind of measurement has been extensively discussed by Asbach et al (2008), including that the instrument can only be reliably used for the size range of nanoparticles between 20 and 100 nm. This leaves the NSAM unable to detect the MSP.

The MEAD uses the same principles as the NSAM, but is smaller and less expensive (Bergamaschi et al., 2012). The articles on the MEAD (Li et al., 2009; Wang et al., 2010) are not clear on the specific particle size range that can be measured, but it seems like the lower detection limit is around 10 nm when looking at their results. This leads to the MEAD not being feasible for detecting the MSP.

Furthermore, Bergamaschi et al. (2012) suggested two instruments that measure the mass concentration of nanoparticles; the Size Selective Sampler (SSS) and the Tapered Element Oscillating Microbalance (TEOM). The SSS is a cascade impactor and is the only device giving a direct estimation of mass concentration with a cut-off frequency around 100 nm, meaning it can measure a total mass above 100 nm or below 100 nm, down to approximately 20 nm (Bergamaschi et al., 2012). As our size of interest is an order of magnitude lower, using this sensor is not feasible. The TEOM measures nano-aerosol mass concentration online with a suitable selective inlet. The main disadvantage is that the TEOM does not provide size information (Bergamaschi et al., 2012). According to NIOSH (2013), the TEOM has size cut-offs at 10, 2.5 and 1 μm, leaving the TEOM too insensitive to detect the MSP.

8 Discussion

This section will discuss the results found in the previous sections concerning the different sensors. This thesis has reviewed 10 different sensors, where most of these were too insensitive to detect particles close to 1 nm and were therefore deemed unfeasible, as this was the main criteria for the sensors. Although the work of Bergamaschi et al. (2012) is eight years old, it gives an indication of what type of instrument might have been improved in the intervening years to be able to detect particles close to 1 nm in radius in the mesosphere. The ELPI might have proven to be an interesting research object, as the sensor could detect particles down to 7 nm and could have been improved further in the intervening years, but it is supposedly very sensitive to field conditions. This sensitivity means the sensor would not be able to operate in the mesosphere, as it contains some of the harshest conditions in the atmosphere. The CPC was the only sensor that could detect particles close to 1 nm in radius, and by extension the SMPS, as it is a combination of a CPC and a DMA. The CPC would have to be modified to endure mesospheric conditions, and some of the problems that arose might be solvable, at least theoretically, including using ice to nucleate onto the MSP, instead of water. Unfortunately, the time needed for the sensor to grow particles was vastly longer then 1 ms, the time the particles would be inside the CPC. Although some problems were solvable theoretically, there is still some uncertainty regarding their response to being operated under field conditions. In particular, the pressure over supercooled water is an approximation and there will have to be performed newer and more conclusive ex-

periments to verify the formula provided by Murphy & Koop (2005). Furthermore, the calculation of the activation radius for condensational growth contains a number of uncertainties, including the aforementioned pressure, the surface energy of ice and the density of supercooled water. The surface energy of ice will most likely be different at 140 K, compared to the surface energy used which was measured at 248 K. The same goes for the density of supercooled water, as the value used in the calculations was based on water at a temperature of 239 K. Finding the surface energy of ice or the supercooled density of water at a temperature of 140 K is a complex and challenging prospect, and could be a thesis unto itself. Additionally, supercooled water will crystallize into ice if disturbed by vibration, which could be challenging to avoid during rocket flight. Having reviewed the different sensors it is therefore possible to conclude that none of these are capable of detecting and measuring MSP in the mesosphere while on-board a rocket.

9 Summary and outlook

The overarching goal of this master thesis was to explore the feasibility of sending a sensor aboard a rocket to detect and determine the composition of the MSP in the mesophere. This thesis presents and assesses various sensors theoretically capable of detecting and measuring particles on the nanometer scale. Having reviewed the various sensors in this thesis, it is now possible to conclude that detecting and measuring the MSP in the mesosphere is not feasible with any of these sensors and instruments, with their current specifications and method of operation. There might be other sensors or instruments that indeed are capable of this already, but they have not been found during the time this thesis was written. Most of the sensors presented here were not sensitive enough to detect the MSP, whilst the CPC, the best candidate, would not be able to measure the MSP, as the particles would not grow fast enough to allow detection, given the limited time the rocket would be in the mesosphere. However, some of these sensors might be able to detect the NLC particles, as they are typically between 5-50 nm in radius, meaning this could be an area of interest for future research. Further research into this subject will have to look at the possibility of speeding up the condensation rate of the CPC, or making more sensitive sensors that can detect particles close to 1 nm in radius, whilst being robust enough to be operable under mesospheric conditions. Additionally, more research regarding the surface energy of ice, the density of supercooled water and the pressure over supercooled water at low temperatures, must be conducted to improve the theoretical framework concerning cloud condensation nuclei and provide more precise calculations. There is also a need for more in-situ observations, more rigorous models that better explain the observations, in addition to a better understanding of quantum physical- and microphysical effects. Furthermore, our understanding of the mesosphere is limited and gaining knowledge about the effects of meteoric smoke particles could be particularly helpful, in order to better understand the phenomenons that take place there. Finally, the longstanding question of how noctilucent clouds are formed might be answered if the composition of the meteoric smoke particles was known. With advances in science and technology, it is most likely a question of when, and not if, there will be technology available that can detect and measure

the MSP in the mesosphere, and thus determine their composition, and, by extension, their other properties.

Acknowledgements

I would like to thank my supervisors, Michael Gausa and Patrick J. Espy for introducing me to an interesting topic, that combined my two main interests in science; space technology and atmospheric physics, for helping me along the way, and for agreeing to be my supervisors. I would also like to thank Vendela Maria Paxal, who introduced me to Michael, which made writing this thesis possible. Furthermore, I would like to thank Adam Balfour, Christina Torgersen and Eirik Ward Hjelvik for many fruitful discussions. Finally, I would like to thank my friends and family for providing me with support and motivation throughout the five years I have spent at NTNU.

References

Ahmed, T. (2010). *Reservoir Engineering Handbook* (4th Ed.). Houston, TX: Gulf Professional Publishing.

Andrews, D. G. (2010). *An Introduction to Atmospheric Physics* (2nd Ed.). Cambridge, UK: Cambridge University Press.

Anthony, J. W., Bideaux, R. A., Bladh, K. W., & Nichols, M. C. (Eds.). (2003). Handbook of Mineralogy, Mineralogical Society of America, Chantilly, VA 20151-1110, USA. Retrieved from http://www.handbookofmineralogy.org/

Atreya, S. K. (1986). *Atmospheres and Ionospheres of the Outer Planets and Their Satellites.* Berlin, Germany: Springer.

Asbach, C., Fissan, H., Stahlmecke, B., Kuhlbusch, T. A., & Pui, D. Y. H. (2009). Conceptual limitations and extensions of lung-deposited Nanoparticle Surface Area Monitor (NSAM). *Journal of Nanoparticle Research, 11*, 101–109. doi: 10.1007/s11051-008-9479-8

Bergamaschi, A., Iavicoli, I., & Savolainen, K. (2012). Exposure Assessment. In B. Fadeel, A. Pietroiusti & A. A. Shvedova (Eds.), *Adverse Effects of Engineered Nanomaterials: Exposure, Toxicology, and Impact on Human Health* (pp. 25-44). Cambridge, MA: Academic Press.

Boinovich, L. B., & Emelyanenko, A. M. (2014). Experimental determination of the surface energy of polycrystalline ice. *Doklady Physical Chemistry, 459*, 198–202. doi: 10.1134/S0012501614120045

Bureau International des Poids et Mesures (BIPM). (2019). A concise summary of the International System of Units, SI. (9th ed.). Retrieved from https://www.bipm.org/utils/common/pdf/si-brochure/SI-Brochure-9-concise-EN.pdf

Campbell, B. A., & Bakhtar, F. (1970). Condensation Phenomena in High Speed Flow of Steam. *Proceedings of the Institution of Mechanical Engineers, 185*(1), 395–405. doi: 10.1243/PIME_PROC_1970_185_047_02

Ceplecha, Z., Borovicka, J., Elford, W. G., Revelle, D. O., Hawkes, R. L., Porubcan, V., & Simek, M. (1998). Meteor phenomena and bodies. *Space Science Review, 84*, 327–471. doi: 10.1023/A:1005069928850

Fentzke, J. T., Janches, D., Strelnikova, I., & Rapp, M. (2009). Meteoric smoke particles derived using dual beam Arecibo UHF observations of D-region spectra during different seasons. *Journal of Atmospheric and Solar–Terrestrial Physics, 71*, 1982–1991. doi: 10.1016/j.jastp.2009.09.002.

Fentzke, J. T., Hsu, V., Brum, C. G. M., Strelnikova, I., Rapp, M., & Nicolls, M. (2012). D region meteoric smoke and neutral temperature retrieval using the poker flat incoherent scatter radar. *Geophysics Research Letters, 39*, L21101. doi: 10.1029/2012GL053841

Fierz, M., Burtscher, H., Steigmeier, P., & Kasper, M. (2008). Field Measurement of Particle Size and Number Concentration with the Diffusion Size Classifier (DiSC). *SAE Technical Paper*. doi: 10.4271/2008-01-1179

Fierz, M., Houle, C., Steigmeier, P., & Burtscher, H. (2011). Design, Calibration, and Field Performance of a Miniature Diffusion Size Classifier. *Aerosol Science and Technology, 45*(1), 1-10. doi: 10.1080/02786826.2010.516283

Guo, S. L., Chen, B. L., & Durrani, S. A. (2012). Solid-State Nuclear Track Detectors. In M. F. L'Annunziata (Ed.), *Handbook of Radioactivity Analysis* (3rd Ed., pp. 233-298). Cambridge, MA: Academic Press. doi: 10.1016/B978-0-12-384873-4.00004-9

Hare, D. E., & Sorensen, C. M. (1987). The density of supercooled water. II. Bulk samples cooled to the homogeneous nucleation limit. *The Journal of Chemical Physics, 87*, 4840. doi: 10.1063/1.453710

Haynes, W. M., Ed. (2011). *CRC Handbook of Chemistry and Physics* (92nd ed.). Boca Raton, FL: CRC Press. ISBN 1439855110.

Hedin, J., Giovane, F., Waldemarsson, T., Gumbel, J., Blum, J., Stroud, R. M., Marlin, L., Moser, J., Siskind, D. E., Jansson, K., Saunders, R. W., Summers, M. E., Reissaus, P., Stegman, J., Plane, J. M. C., & Horányi, M. (2014). The MAGIC meteoric smoke particle sampler. *Journal of Atmospheric and Solar-Terrestrial Physics, 118*, 127-148. doi: 10.1016/j.jastp.2014.03.003

Hering, S. V., Lewis, G. S., Spielman, S. R., & Eiguren-Fernandez, A. (2019). A MAGIC concept for self-sustained, water-based, ultrafine particle counting. *Aerosol Science and Technology, 53*(1), 63-72. doi: 10.1080/02786826.2018.1538549

Hering, S. V., Lewis, G. S., Spielman, S. R., Eiguren-Fernandez, A., Kreisberg, N. M., Kuang, C., & Attoui, M. (2017). Detection near 1-nm with a laminar-flow, water-based condensation particle counter. *Aerosol Science and Technology, 51*(3), 354-362. doi: 10.1080/02786826.2016.1262531

Hervig, M. E., Deaver, L. E., Bardeen, C. G., Russell III, J. M., Bailey, S. M., & Gordley, L. L. (2012). The content and composition of meteoric smoke in mesospheric ice particles from SOFIE observations. *Journal of Atmospheric and Solar-Terrestrial Physics, 84-85*, 1-6. doi: 10.1016/j.jastp.2012.04.005

Hunten, D. M., Turco R. P., & Toon, O, B. (1980). Smoke and Dust Particles of Meteoric Origin in the Mesosphere and Stratosphere. *Journal of Atmospheric Sciences, 37*, 1342-1357. doi: 10.1175/1520-0469(1980)037<1342:SADPOM>2.0.CO;2

Industrial Laser Solutions. (2014, January 10). Pyroelectric energy sensor. Retrieved from https://www.industrial-lasers.com/home/article/16488058/pyroelectric-energy-sensor

International Association for the Properties of Water and Steam (IAPWS). (2014). Revised Release on Surface Tension of Ordinary Water Substance. Retrieved from: http://www.iapws.org/relguide/Surf-H2O-2014.pdf

Kaszuba, M., McKnight, D., Connah, M. T., McNeil-Watson, F. K., & Nobbmann, U. (2008) Measuring sub nanometre sizes using dynamic light scattering. *Journal of Nanoparticle Research, 10*, 823–829. doi: 10.1007/s11051-007-9317-4

Lenntech. (2020). Molecular Weight Calculator. Retrieved from https://www.lenntech.com/calculators/molecular/molecular-weight-calculator.htm

Li, L., Chen, D., & Tsai, P. (2009). Use of an electrical aerosol detector (EAD) for nanoparticle size distribution measurement. *Journal of Nanoparticle Research, 11*, 111–120. doi: 10.1007/s11051-008-9418-8

Lide, D. R., Ed. (1992). *CRC Handbook of Chemistry and Physics* (73rd ed.). Boca Raton, FL: CRC Press.

Lide, D. R., Ed. (2003). *CRC Handbook of Chemistry and Physics* (84th ed.). Boca Raton, FL: CRC Press. ISBN 9780849304842.

Lide, D. R., Ed. (2005). *CRC Handbook of Chemistry and Physics* (86th ed.). Boca Raton, FL: CRC Press. ISBN 0-8493-0486-5.

Megner, L. (2008). *Meteoric Aerosols in the Midddle Atmosphere* (Doctoral Thesis). Stockholm University, Stockholm.

Mills, A. F., & Seban, R. A. (1967). The condensation coefficient of water. *International Journal of Heat and Mass Transfer, 10*(12), 1815-1827, doi: 10.1016/0017-9310(67)90052-X

Murphy, D. M., & Koop, T. (2005). Review of the vapour pressures of ice and supercooled water for atmospheric applications. *Quarterly Journal of the Royal Meteorological Society, 131*(608), 1539-1565. doi: 10.1256/qj.04.94

Murray, B. J., O'Sullivan, D., Atkinson, J. D., & Webb, M. E. (2012). Ice nucleation by particles immersed in supercooled cloud droplets. *Chemical Society Reviews, 41*, 6519-6554. doi: 10.1039/C2CS35200A

NASA. (2000). NRLMSISE-00 Atmosphere Model. Retrieved from https://ccmc.gsfc.nasa.gov/modelweb/models/nrlmsise00.php

NIOSH. (2013). *Current strategies for engineering controls in nanomaterial production and downstream handling processes* (Publication No. 2014–102). Retrieved from https://www.cdc.gov/niosh/docs/2014-102/pdfs/2014-102.pdf?id=10.26616/NIOSHPUB2014102

Ophir Photonics, (2013, August 18). *Sensors for Measuring Laser Energy* [Video]. Retrieved from https://www.ophiropt.com/laser–measurement/laser-power-energy-meters/products/Laser-Pyroelectric-Energy-Sensors/Pyroelectric-Laser-Energy-Sensors

Picone, J. M., Hedin, A. E., Drob. D. P., & Aikin, A. C. (2002). NRLMSISE-00 empirical model of the atmosphere: Statistical comparisons and scientific issues. *Journal of Geophysical Research: Space Physics, 107*(A12). doi: 10.1029/2002JA009430

Plane, J. M. C. (2012). Cosmic dust in the earth's atmosphere. *Chemical Society Review, 41*, 6507-6518. doi: 10.1039/c2cs35132c

Plane, J. M. C., Feng, W., & Dawkins, E. C. M. (2015). The Mesosphere and Metals: Chemistry and Changes. *Chemical Reviews, 115*(10), 4497-4541. doi: 10.1021/cr500501m

Rapp, M., & Thomas, G. E. (2006). Review: Modeling the microphysics of mesospheric ice particles: Assessment of current capabilities and basic sensitivities. *Journal of Atmospheric and Solar-Terrestrial Physics, 68*(7), 715–744. doi: 10.1016/j.jastp.2005.10.015

Rapp, M., Strelnikova, I., & Gumbel, J. (2007). Meteoric smoke particles: Evidence from rocket and radar techniques. *Advances in Space Research, 40*(6), 809-817. doi: 10.1016/j.asr.2006.11.021

Robertson, S., Dickson, S., Horányi, M., Sternovsky, Z., Friedrich, M., Janches, D., Megner, L., & Williams, B. (2014). Detection of meteoric smoke particles in the mesosphere by a rocket-borne mass spectrometer. *Journal of Atmospheric and Solar-Terrestrial Physics, 118*, 161-179. doi: 10.1016/j.jastp.2013.07.007

Rosinski, J., & Snow, R.H. 1961. Secondary particulate matter from meteor vapors. *Journal of Meteorology, 18*, 736–745. doi: 10.1175/1520-0469(1961)018<0736:SPMFMV>2.0.CO;2

Sissenwine, N., Grantham, D. D., & Salmela, H. A. (1968). *Humidity up to the mesopause* (Air Force Surveys in Geophysics No. 206). Bedford, MA: Air Force Cambridge Research Laboratories. Retrieved from: https://apps.dtic.mil/sti/citations/AD0679996

SlideModel. (2019). Atmosphere Layeres PowerPoint Template. Retrieved from https://slidemodel.com/templates/atmosphere-layers-powerpoint-template/

Speight, J. G. (2017). *Environmental Organic Chemistry for Engineers.* Oxford, UK: Butterworth-Heinemann.

Strelnikova, I., Rapp, M., Raizada, S. & Sulzer, M. (2007). Meteor smoke particle properties derived from Arecibo incoherent scatter radar observations. *Geophysical Research Letters, 34*. doi: 10.1029/2007GL030635

The University Corporation for Atmospheric Research (UCAR). (2011). The exosphere - overview. Retrieved from https://scied.ucar.edu/shortcontent/exosphere-overview

The University Corporation for Atmospheric Research (UCAR). (2008). The mesosphere - overview. Retrieved from https://scied.ucar.edu/shortcontent/mesosphere-overview

Turco, R. P., Toon, O. B., Qhitten, R. C., Keesee, R. G., & Hollenbach, D. (1982). Noctilucent clouds: simulation studies of their genesis, properties and global influence. *Planetary and Space Science, 30*, 1147-1181. doi: 10.1016/0032-0633(82)90126-X

Varney, R. H., & Kelley, M. C. (2015). MESOSPHERE | Polar Summer Mesopause. In: G. R. North, J. Pyle & F. Zhang (Eds.), *Encyclopedia of Atmospheric Sciences* (2nd Ed.). Cambridge, MA: Academic Press.

Viisanen, Y., Strey, R., & Reiss, H. (1993). Homogeneous nucleation rates for water. *The Journal of Chemical Physics, 99*, 4680. doi: 10.1063/1.466066

Wang, Y. F., Tsai, P. J., Chen, C. W., Chen, D. R., & Hsu, D. J. (2010). Using a Modified Electrical Aerosol Detector To Predict Nanoparticle Exposures to Different Regions of the Respiratory Tract for Workers in a Carbon Black Manufacturing Industry. *Environmental Science & Technology, 44*(17), 6767-6774. doi: 10.1021/es1010175

Zhang, C., Zhu, R., & Yang, W. (2016). A Micro Aerosol Sensor for the Measurement of Airborne Ultrafine Particles. *Sensors (Basel, Switzerland), 16*(3), 399. doi: 10.3390/s16030399

Appendix A - Overview of rejected sensors

Type of sensor	Reason for rejection	Reference
Electromobility spectrometer	Time resolution	Winklmayr et al. (1991)
DMA	Detection cut-off	Kelly & McMurry (1992)
Hydrazine Chemical Sensor	Detection cut-off	Kim et al. (2015)
Partector 2	Particle size range	Naneos (2020)
Micro Aerosol Sensor	Particle size range	Zhang et al. (2016)
Air pollution monitor	Particle size range	Su (2018)
Dynamic light scattering	Requires a sample	Kaszuba et al. (2008)
Pegasor Particle Sensor	Measures charged particles	Amanatidis et al. (2016)
Thymine Sensor	Measures charged particles	Yang et al. (2017)
Suprathermal Plasma Imager	Measures charged particles	Knudsen et al. (2003)
TSI 3772	Size of sensor	Kangasluoma et al. (2015)
Airmodus A20	Size of sensor	Kangasluoma et al. (2015)

Table 2: A table listing various sensors and instruments that were considered and disregarded as not being capable of detecting the MSP in the mesosphere. The full references can be found below.

References

Amanatidis, S., Maricq, M. M., Ntziachristos, L., & Samaras, Z. (2016). Measuring number, mass, and size of exhaust particles with diffusion chargers: The dual Pegasor Particle Sensor. *Journal of Aerosol Science, 92*, 1-15. doi: 10.1016/j.jaerosci.2015.10.005

Kangasluoma, J., Ahonen, L., Attoui, M., Vuollekoski, H., Kulmala M., & Petäjä, T. (2015) Sub-3 nm Particle Detection with Commercial TSI 3772 and Airmodus A20 Fine Condensation Particle Counters. *Aerosol Science and Technology, 49*(8). 674-681. doi: 10.1080/02786826.2015.1058481

Kaszuba, M., McKnight, D., Connah, M. T., McNeil-Watson, F. K., & Nobbmann, U. (2008) Measuring sub nanometre sizes using dynamic light scattering. *Journal of Nanoparticle Research, 10*, 823–829. doi: 10.1007/s11051-007-9317-4

Kelly, W. P., & McMurry, P. H. (1992). Measurement of Particle Density by Inertial Classification of Differential Mobility Analyzer–Generated Monodisperse Aerosols. *Aerosol Science and Technology, 17*(3), 199-212. doi: 10.1080/02786829208959571

Kim, S. P., Lee, S. G., Choi, M. Y., & Choi, H. C. (2015). Highly Sensitive Hydrazine Chemical Sensor Based on CNT-PdPt Nanocomposites. *Journal of Nanomaterials*. doi: doi.org/10.1155/2015/120485

Knudsen, D. J., Burchill, J. K., Berg, K., Cameron, T., Enno, G. A., Marcellus, C. G., King, E. P., & Wevers, I. (2003). A low-energy charged particle distribution imager with a compact sensor for space applications. *Review of Scientific Instruments, 74*(202). doi: 10.1063/1.1525869

Naneos. (2020). Partector 2: The world's smallest multimetric nanoparticle detector. Retrieved from: https://www.naneos.ch/partector2.html

Su, J. (2018). Portable and sensitive air pollution monitoring. *Light Science & Applications, 7*(3). doi: 10.1038/s41377-018-0017-x

Winklmayr, W., Reischl, G. P., Lindner A. O., & Berner, A. (1991). A new electromobility spectrometer for the measurement of aerosol size distributions in the size range from 1 to 1000 nm. *Journal of Aerosol Science, 22*(3), 289-296. doi:10.1016/S0021-8502(05)80007-2

Yang, H., Ye, S. B., Fu, Y., Zhang, W., Xie, F., Gong, L., Fang, P. P., Chen, J., & Tong, Y. (2017). A Simple and Highly Sensitive Thymine Sensor for Mercury Ion Detection Based on Surface Enhanced Raman Spectroscopy and the Mechanism Study. *Nanomaterials, 7*(7), 192. doi: 10.3390/nano7070192

Zhang, C., Zhu, R., & Yang, W. (2016). A Micro Aerosol Sensor for the Measurement of Airborne Ultrafine Particles. *Sensors (Basel, Switzerland), 16*(3), 399. doi: 10.3390/s16030399